Journal of Physics:
Conference Series

PAPER • **OPEN ACCESS**

On the critical velocity of a mass moving along an infinite beam supported by three viscoelastic layers

To cite this article: Z Dimitrovová and T Mazilu 2024 *J. Phys.: Conf. Ser.* **2647** 252017

Journal of Physics: Conference Series **2647** (2024) 252017 doi:10.1088/1742-6596/2647/25/252017

On the critical velocity of a mass moving along an infinite beam supported by three viscoelastic layers

Z Dimitrovová[1,2] and T Mazilu[3]

[1]Department of Civil Engineering, NOVA School of Science and Technology, NOVA University of Lisbon, Lisbon, Portugal
[2]IDMEC, Instituto Superior Técnico, Universidade de Lisboa, Lisbon, Portugal
[3]Department of Railway Vehicles, Faculty of Transport, National University of Science and Technology Politehnica Bucharest
traian.mazilu@upb.ro

Abstract. Numerical assessment of the dynamic behaviour of structures subject to moving loads are under huge development, as are other approaches, to mention e.g. (semi)analytical methods and methods based on frequency-domain moving Green's function. This contribution is focused on an infinite beam supported by three viscoelastic layers, which, due to its computational efficiency and relatively good approximation of reality, is a quite common model of a railway line. New developments that are presented concern the instability of a moving mass. The critical velocity in this context will be used for the lowest velocity that separates stable and unstable behaviour. The two above-mentioned methods are compared in terms of computational efficiency and accuracy of the obtained results. All results are presented in dimensionless form to cover a wide range of possible scenarios. When the frequency-domain moving Green's function is used to calculate the critical velocity via D-decomposition method, then a little damping should be considered for numerical stability. The semianalytical approach, on the other hand, can deal with both undamped and damped structures without any problems. Nevertheless, the final results obtained by the two methods (in the Green's function approach under the assumption of very low damping) are identical.

1. Introduction

Moving load problems focusing on vehicle stability in railway applications have belonged to an active scientific field for already many decades. Several models of the moving object as well as of the supporting elastic structure have already been used. A railway vehicle can be simplified as one [1-3] or two moving masses [4,5]; one two-mass [6,7] or three-body [8,9] oscillator or a train of moving objects [10-13]. A more detailed vehicle model is introduced in [14-15]. The track is usually modelled by an Euler-Bernoulli infinite beam placed on a supporting structure, which can be in form of one [1,2,4,16], two [5] or three [17,18] elastic layers. The Timoshenko beam can also be used [8,19] to improve the beam model. Instead of continuous supports, discrete supports are implemented in [20]. In addition, the moving element method [21,22], a new moving beam element [23] or the model incorporating a nonlinear dynamic interaction [24], as well as papers accounting for large deformations [25], can also be mentioned.

This contribution is concerned with an infinite beam supported by three viscoelastic layers, which is a quite common model of a railway line. The subject of interest is the critical velocity defined as the lowest possible velocity marking the separation between stable and unstable behaviour of one moving mass traversing the structure by a constant velocity.

In Section 2, the model is presented together with the simplifications introduced and the basic assumptions adopted. The governing equations are stated, and solutions are presented by the two analysed methods in Sections 3 and 4. The model is conveniently described by a set of dimensionless parameters, for which a range of possible numerical values is derived. The obtained results are demonstrated on a set of selected cases in Section 5. It turns out that there are several cases with quite unpredictable behaviour, namely when very low damping levels are introduced. In the semianalytical approach, the so-called lines of instability are tracked as a function of the ratios of the velocity and of the moving mass, [5,17]. It is shown that there are several such lines. They can have a rather strange evolution, because for some parameter combinations they can be closed. However, in most cases they end with asymptotes tending to an infinite mass ratio for a specific velocity ratio. Additionally, there is always at least one branch which tends to zero mass ratio for an infinite velocity ratio. Instability lines determination can be conducted within the real domain demonstrating the easiness of implementation. It is also demonstrated that the expected association to the moving force critical velocity is only fulfilled in some cases. This is due to the fact that there are not always three values of such a critical velocity. When only one exists, then the others are replaced by pseudocritical velocities, which can be dominant or not. The level of dominance is influencing their correct determination and effect on instability lines. Further, especially at low damping, instability branches have more vertical asymptotes, than such three critical velocities indicate. It is worthwhile to remark that in several cases the critical velocity of the moving force can be determined analytically.

Some results have been verified using a different method, namely the D-decomposition method applied in terms of Green's function [10]. The undamped cases have been excluded due to numerical instability. However, the results obtained using the two methods are identical when a little damping is considered.

2. Computational model

The railway track model composed of three viscoelastic layers is widely used to determine the dynamic response of ballasted tracks under moving loads due to its computational efficiency. It consists of a beam representing the rail, several spring/damper elements and point masses. Point mases stand for half sleepers and the ballast that is dynamically activated. Spring/damper elements model all resilient layers, such as the rail pads, the ballast and finally the foundation. They are also used to represent the ballast shear stiffness, [18]. Realistic values of ballast contribution can be determined either by experiments or analytically by exploiting the ballast stress cone theory.

A model subjected to one moving mass on which a constant force acts is depicted in figure 1.

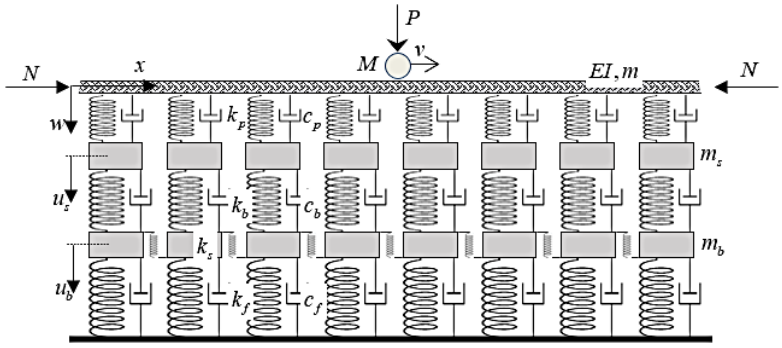

Figure 1. The model of the railway track subjected to a moving mass, [18].

One of the main assumptions that greatly facilitates the solution approaches discussed in this paper is that the supports are assumed to be continuous. This is not a major limitation as the differences between the behaviour of the model with discrete and continuous supports would only be noticeable for high frequencies close to the pinned-pinned frequency. Furthermore, the effect of discrete supports can be modelled using by adding a harmonic component to the moving force.

The governing equations can be written in the following way, [17,18]

$$\begin{aligned}
&EIw_{,xxxx} + Nw_{,xx} + mw_{,tt} + c_p\left(w_{,t} - u_{s,t}\right) + k_p\left(w - u_s\right) = p \\
&m_s u_{s,tt} - c_p\left(w_{,t} - u_{s,t}\right) - k_p\left(w - u_s\right) + c_b\left(u_{s,t} - u_{b,t}\right) + k_b\left(u_s - u_b\right) = 0 \\
&m_b u_{b,tt} - k_s u_{b,xx} - c_b\left(u_{s,t} - u_{b,t}\right) - k_b\left(u_s - u_b\right) + c_f u_{b,t} + k_f u_b = 0
\end{aligned} \tag{1}$$

where all parameters which appear in figure 1 as discrete entities are already assumed in their distributed form, assuring that the model is longitudinally homogeneous. The model is thus characterized by the beam bending stiffness EI and mass per unit length m; rail pads, defined by their vertical stiffness k_p and viscous damping c_p; sleepers introduced as point masses m_s; ballast layer, modelled by its vertical and shear stiffness k_s, k_b, viscous damping c_b and dynamically activated mass m_b; foundation described by its vertical stiffness k_f and viscous damping c_f. As regard the load, in addition to a constant moving mass M acted by a constant force P, an axial force N can be applied. The velocity v is also constant and the objective of the analysis is to solve the deflection fields w, u_s, u_b assumed positive when acting downward, same as the force P. For the situation described above, the loading term is

$$p(x,t) = \left(P - Mw_{0,tt}(t)\right)\delta(x - vt) \tag{2}$$

To obtain a solution of the system (1), (2), first, w_0 is removed by considering a tight contact, that is $w_0(t) = w(vt,t)$. Further, moving coordinate is introduced by $r = x - vt$. Then, dimensionless parameters are used, definition of which is linked to a representative Winkler beam with EI, m, k_f and c_f. These parameters are listed in the following equations.

$$\tilde{w} = \frac{w}{w_{st}},\ \tilde{u}_s = \frac{u_s}{w_{st}},\ \tilde{u}_b = \frac{u_b}{w_{st}} \text{ with } w_{st} = \frac{P\chi}{2k_f} \text{ and } \chi = \sqrt[4]{\frac{k_f}{4EI}} \tag{3}$$

$$\alpha = \frac{v}{v_{ref}} \text{ with } v_{ref} = \sqrt[4]{\frac{4k_f EI}{m^2}} = \frac{1}{\chi}\sqrt{\frac{k_f}{m}},\ \xi = \chi r,\ \tau = \chi v_{ref} t \tag{4}$$

$$\mu_s = \frac{m_s}{m},\ \mu_b = \frac{m_b}{m},\ \kappa_p = \frac{k_p}{k_f},\ \kappa_b = \frac{k_b}{k_f} \tag{5}$$

$$\eta_p = \frac{c_p}{2\sqrt{mk_f}},\ \eta_b = \frac{c_b}{2\sqrt{mk_f}},\ \eta_f = \frac{c_f}{2\sqrt{mk_f}},\ \eta_N = \frac{N}{2\sqrt{k_f EI}},\ \eta_s = \frac{k_s}{2\sqrt{k_f EI}} \tag{6}$$

where $\tilde{w}, \tilde{u}_s, \tilde{u}_b, \xi, \tau$ are dimensionless unknown displacements, spatial coordinate and time, respectively. Homogeneous initial conditions and usual boundary conditions for infinite structures are assumed.

3. Semianalytical approach

In order to obtain the solution of the problem, firstly the Laplace transform is applied and then the Fourier one. The set of governing equations is then more conveniently written in a matrix form as

$$\begin{bmatrix} D_1 + D_2 & -D_2 & 0 \\ -D_2 & D_2 + D_3 + D_4 & -D_4 \\ 0 & -D_4 & D_4 + D_5 + D_6 + D_7 \end{bmatrix} \begin{Bmatrix} W \\ V \\ U \end{Bmatrix} = \begin{Bmatrix} 2\eta_C / \mathrm{i}q + \eta_M q^2 \tilde{W}(0,q) \\ 0 \\ 0 \end{Bmatrix} \tag{7}$$

where W, V, U are the unknown displacements in the transformed space and

$$D_1(p,q) = p^4/4 - (q-\alpha p)^2 - \eta_N p^2,\ D_2(p,q) = 2\mathrm{i}\eta_p(q-\alpha p) + \kappa_p \tag{8}$$

$$D_3(p,q) = -\mu_s(q-\alpha p)^2,\ D_4(p,q) = 2\mathrm{i}\eta_b(q-\alpha p) + \kappa_b \tag{9}$$

$$D_5(p,q) = -\mu_b(q-\alpha p)^2,\ D_6(p,q) = 2\mathrm{i}\eta_f(q-\alpha p) + 1,\ D_7(p,q) = \eta_s p^2 \tag{10}$$

It is of note that the Laplace image of τ is $\bar{q} = \mathrm{i}q$, where q is frequency, however $\bar{q}$ is used in the definition to maintain the correct formalism. The Fourier counterpart of ξ is p. On the right-hand side of Eq. (7), $\tilde{W}(0,q)$ is still only a Laplace image of the beam deflection at the active point and must be eliminated. Further ratios of the moving force and mass are

$$\eta_M = \frac{M\chi}{m},\ \eta_C = \frac{P}{P} \tag{11}$$

The moving force ratio seems unnecessary, but it is mathematically more correct and better suitable for further generalizations. First, the governing equations must be solved for $W(p,q)$

$$W(p,q) = \frac{d_2}{d_3}\left(\frac{2\eta_C}{\mathrm{i}q} + \eta_M q^2 \tilde{W}(0,q)\right) \tag{12}$$

where d_3 is the determinant of the whole system and d_2 is the subdeterminant obtained when the first row and the first column of d_3 are cut. Then, one can perform the inverse Fourier transform to retrieve the Laplace image

$$\tilde{W}(\xi,q) = \frac{4\eta_C}{\mathrm{i}q\left(\pi - 2\eta_M q^2 K(0,q)\right)} K(\xi,q) \text{ with } K(\xi,q) = \int_{-\infty}^{\infty} \frac{d_2}{d_3} \mathrm{e}^{\mathrm{i}p\xi} \mathrm{d}p \tag{13}$$

Solution in the Fourier space is thus analytical. Inverse Laplace transform is performed as much as possible by contour integration. It is convenient to switch the coordinates and perform the inverse transform as indicated below.

$$\tilde{w}(\xi,\tau) = \frac{1}{\pi} \int_{-\mathrm{i}a-\infty}^{-\mathrm{i}a+\infty} \frac{-2\mathrm{i}\eta_C K(\xi,q)}{q\left(\pi - 2\eta_M q^2 K(0,q)\right)} \mathrm{e}^{\mathrm{i}q\tau} \mathrm{d}q \tag{14}$$

where a is selected so that below the line $(-\mathrm{i}a - \infty, -\mathrm{i}a + \infty)$ in the complex q-plane there are no discontinuities or poles of the function to be integrated More details can be found in previous works related to similar models, [5,17,18].

4. D-decomposition method based on Green's function

The Laplace transformed governing equations in dimensionless form in moving coordinate system can be written as

$$\mathbf{L}_{\xi,\bar{q}} \tilde{\mathbf{q}} = \tilde{\mathbf{p}}_{\xi,\bar{q}} \tag{15}$$

where $\tilde{\mathbf{q}} = [W(\xi,\bar{q}) \quad V(\xi,\bar{q}) \quad U(\xi,\bar{q})]$ are the Laplace transform of $\tilde{w}(\xi,\tau)$, $\tilde{u}_s(\xi,\tau)$, $\tilde{u}_b(\xi,\tau)$ via the Laplace transform, $\mathbf{L}_{\xi,\bar{q}}$ stands for the matrix differential operator

$$\mathbf{L}_{\xi,\bar{q}} = \begin{bmatrix} L_{\xi,\bar{q},11} & L_{\xi,\bar{q},12} & 0 \\ L_{\xi,\bar{q},21} & L_{\xi,\bar{q},22} & L_{\xi,\bar{q},23} \\ 0 & L_{\xi,\bar{q},32} & L_{\xi,\bar{q},33} \end{bmatrix} \tag{16}$$

with

Journal of Physics: Conference Series **2647** (2024) 252017 doi:10.1088/1742-6596/2647/25/252017

$$\begin{aligned}
&\mathrm{L}_{\xi,\bar{q},11} = \mathrm{D}_\xi^4 + 4(\eta_N + \alpha^2)\mathrm{D}_\xi^2 + 4\bar{q}^2 - 8\alpha s \mathrm{D}_\xi - 8\alpha\eta_p \mathrm{D}_\xi + 8\eta_p \bar{q} + 4\kappa_p \\
&\mathrm{L}_{\xi,\bar{q},12} = 8\alpha\eta_p \mathrm{D}_\xi - 8\eta_p \bar{q} - 4\kappa_p \\
&\mathrm{L}_{\xi,\bar{q},21} = 2\alpha\eta_p \mathrm{D}_\xi - 2\eta_p \bar{q} - \kappa_p \\
&\mathrm{L}_{\xi,\bar{q},22} = \alpha^2\mu_s \mathrm{D}_\xi^2 + \mu_s \bar{q}^2 - 2\alpha\mu_s \bar{q}\mathrm{D}_\xi - 2\alpha(\eta_p + \eta_b)\mathrm{D}_\xi + 2(\eta_p + \eta_b)\bar{q} + \kappa_p + \kappa_b \\
&\mathrm{L}_{\xi,\bar{q},23} = 2\alpha\eta_b \mathrm{D}_\xi - 2\eta_b \bar{q} - \kappa_b \\
&\mathrm{L}_{\xi,\bar{q},32} = L_{\xi,s,23} \\
&\mathrm{L}_{\xi,\bar{q},33} = (\alpha^2\mu_b - \eta_s)\mathrm{D}_\xi^2 + \mu_b \bar{q}^2 - 2\alpha\mu_b \bar{q}\mathrm{D}_\xi - 2\alpha(\eta_b + \eta_f)\mathrm{D}_\xi + 2(\eta_b + \eta_f)\bar{q} + \kappa_b + 1
\end{aligned} \tag{17}$$

where $\mathrm{D}_\xi^n = \mathrm{d}^n / \mathrm{d}\xi^n$ and $\tilde{\mathbf{p}}_{\xi,\bar{q}} = \left[-4\eta_M \bar{q}^2 W(0,\bar{q})\delta(\xi) \quad 0 \quad 0\right]^t$.

Multiplying Eq. (15) by the adjoint matrix of the matrix differential operator $\mathbf{L}_{\xi,\bar{q}}$, it holds

$$\mathrm{diag}(\Delta,\Delta,\Delta)\tilde{\mathbf{q}} = \tilde{\mathbf{f}} \tag{18}$$

where Δ is the differential operator given by

$$\Delta = \sum_{j=0}^{8} a_j \mathrm{D}_\xi^{8-j} \tag{19}$$

where a_j are coefficients depending on the velocity ratio α and $\bar{q}$ coordinate, and

$$\tilde{\mathbf{f}} = \mathbf{L}^*_{\xi,\bar{q}} \tilde{\mathbf{p}}_{\xi,\bar{q}} \tag{20}$$

where $\mathbf{L}^*_{\xi,\bar{q}}$ stands for the adjoint matrix of the matrix differential operator $\mathbf{L}_{\xi,\bar{q}}$

$$\mathbf{L}^*_{\xi,\bar{q}} = \begin{bmatrix} L_{\xi,\bar{q},22}L_{\xi,\bar{q},33} - L_{\xi,\bar{q},23}L_{\xi,\bar{q},32} & -L_{\xi,\bar{q},12}L_{\xi,\bar{q},33} & L_{\xi,\bar{q},12}L_{\xi,\bar{q},23} \\ -L_{\xi,\bar{q},21}L_{\xi,\bar{q},33} & L_{\xi,\bar{q},11}L_{\xi,\bar{q},33} & -L_{\xi,\bar{q},11}L_{\xi,\bar{q},23} \\ L_{\xi,\bar{q},21}L_{\xi,\bar{q},32} & -L_{\xi,\bar{q},11}L_{\xi,\bar{q},32} & L_{\xi,\bar{q},11}L_{\xi,\bar{q},22} - L_{\xi,\bar{q},12}L_{\xi,\bar{q},21} \end{bmatrix} \tag{21}$$

It can be observed that the first equation of Eq. (22) is independent upon the other two

$$\Delta \cdot W(\xi,\bar{q}) = -4\eta_M \bar{q}^2 R_{\xi,\bar{q}} W(0,\bar{q})\delta(\xi) \tag{22}$$

where the differential operator $R_{\xi,\bar{q}}$ has the form

$$R_{\xi,\bar{q}} = L_{\xi,\bar{q},22}L_{\xi,\bar{q},33} - L_{\xi,\bar{q},23}L_{\xi,\bar{q},32} = \sum_{j=0}^{4} r_j D_\xi^{4-j} \tag{23}$$

where r_j are coefficients depending on the velocity ratio α and $\bar{q}$ coordinate.

Solution of Eq. (26) is

$$W(\xi,\bar{q}) = -4\eta_M \bar{q}^2 W(0,\bar{q}) \int_{-\infty}^{\infty} G_\Delta(\xi,\varepsilon) R_{\xi,\bar{q}} \delta(\varepsilon)\mathrm{d}\varepsilon \tag{24}$$

where $G_\Delta(\xi, \varepsilon)$ is Green's function associated to Δ.

Considering $\xi = 0$, one obtains

$$W(0,\bar{q})\left[1 + 4\eta_M \bar{q}^2 \int_{-\infty}^{\infty} G_\Delta(0,\varepsilon) R_{\xi,\bar{q}} \delta(\varepsilon)\mathrm{d}\varepsilon\right] = 0 \tag{25}$$

or

$$W(0,\bar{q})\left[1 + 4\eta_M \bar{q}^2 \sum_{i=0}^{4} r_i (-1)^{4-i} \frac{\partial^{4-i} G_H(0,0)}{\partial \varepsilon^{4-i}}\right] = 0 \tag{26}$$

The characteristic equation emerges from Eq. (26)

$$1 + 4\eta_M \bar{q}^2 \sum_{i=0}^{4} r_i (-1)^{4-i} \frac{\partial^{4-i} G_\Delta(0,0)}{\partial \varepsilon^{4-i}} = 0, \tag{27}$$

Journal of Physics: Conference Series **2647** (2024) 252017 doi:10.1088/1742-6596/2647/25/252017

Green's function $G_\Delta(\xi,\varepsilon)$ can be built in the form

$$G_\Delta(\xi,\varepsilon)=\begin{cases} G_\Delta^-(\xi,\varepsilon)=\dfrac{1}{a_0}\displaystyle\sum_{i=1}^{n}\dfrac{e^{\lambda_i(\xi-\varepsilon)}}{\prod\limits_{\substack{k=1\\k\neq i}}^{8}(\lambda_k-\lambda_i)} & -\infty<\xi<\varepsilon \\ G_\Delta^+(\xi,\varepsilon)=-\dfrac{1}{a_0}\displaystyle\sum_{i=n+1}^{8}\dfrac{e^{\lambda_i(\xi-\varepsilon)}}{\prod\limits_{\substack{k=1\\k\neq i}}^{8}(\lambda_k-\lambda_i)} & \varepsilon<\xi<\infty, \end{cases} \tag{28}$$

where λ_i is the eigenvalue and Re $\lambda_i > 0$ for $i = 1$ to n and Re $\lambda_i < 0$ for $i = n + 1$ to 8.

Finally, equation (27) is reformulated as follows

$$z(\bar{q},\alpha)=1 \tag{29}$$

where $z(\bar{q},\alpha)$ is given by

$$z(\bar{q},\alpha)=-4\frac{\eta_M\bar{q}^2}{a_0}\sum_{i=1}^{n}\frac{\sum\limits_{j=0}^{4}r_j\lambda_i^{4-j}}{\prod\limits_{\substack{k=1\\k\neq i}}^{8}(\lambda_k-\lambda_i)} \tag{30}$$

Stability of a moving mass along the three-layer model via the Green's function approach and D-decomposition method can be reflected in terms of the critical velocity which is the velocity at which the equilibrium point is simple stable. This equilibrium point shifts its character depending on the velocity as follows: at lower velocity than the critical velocity, this is asymptotically stable, and at higher velocity, the equilibrium point becomes unstable. Stability of the equilibrium point of the moving mass – beam on three-layer system is related to the roots of the characteristic equation.

D-decomposition method can be applied following the rule: given velocity of the moving mass, curves (Re $z(\pm iq)$, Im $z(\pm iq)$) and (Re $z(\delta \pm iq)$, Im $z(\delta \pm iq)$) with $\delta > 0$ are drawn in the complex plane. Curve (Re $z(\pm iq)$, Im $z(\pm iq)$) shares the complex plane into stable and unstable part, and the curve (Re $z(\delta \pm iq)$, Im $z(\delta \pm iq)$) shows which side is the unstable part of the complex plan. The system is stable if the point (1,0) is on the stable part (see figure 2a)) and unstable otherwise (see figure 2b)). In the case of figure 2, the stable part of the complex plane is to the right of the curve (Re $z(\pm iq)$, Im $z(\pm iq)$), but the opposite can also happen (figure 3).

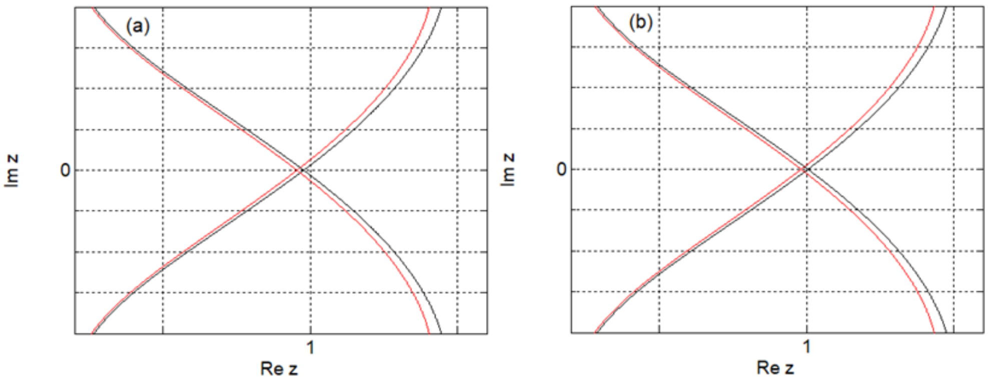

Figure 2. Explanatory on how the D-decomposition method is applied: a) stable; b) unstable; —, (Re $z(\pm iq)$, Im $z(\pm iq)$); —, (Re $z(\delta \pm iq)$, Im $z(\delta \pm iq)$).

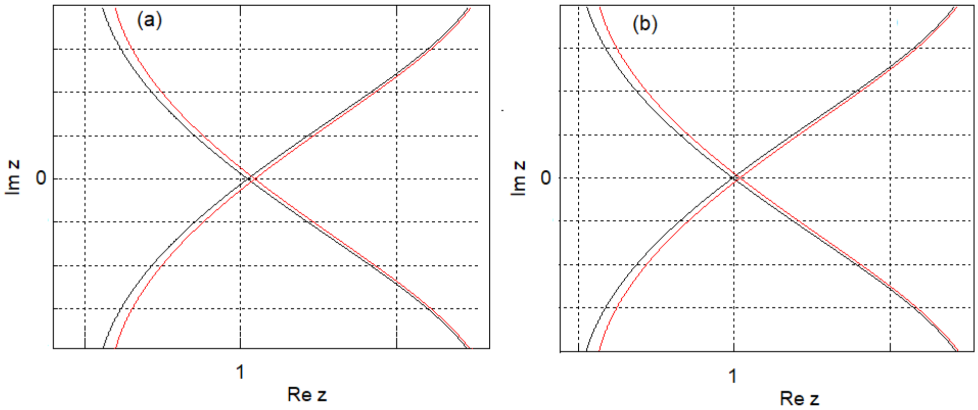

Figure 3. Explanatory on how the D-decomposition method is applied: a) stable; b) unstable; —, (Re $z(\pm iq)$, Im $z(\pm iq)$); —, (Re $z(\delta \pm iq)$, Im $z(\delta \pm iq)$).

5. Examples

All results will be presented in their dimensionless form using the parameters defined in Eqs. (5) and (6), so that they will be valid for a wide range of possible cases. To achieve this, admissible ranges of true values are identified and then the dimensionless values fit into reasonable intervals, as:

$$\mu_s = 1 \div 6\,,\ \mu_b = 2.5 \div 50\,,\ \kappa_p = 0.03 \div 50000\,,\ \kappa_b = 0.1 \div 10000\,,\ \eta_s = 0 \div 100 \qquad (31)$$

However, academic values for η_M will also be used to illustrate better instability branches behaviour. Damping ratios will be indicated directly without connection to real values, because their ranges are very uncertain.

For demonstration purposes five cases have been selected. Input data are summarized in table 1.

Table 1. Definition of test cases.

Case	μ_s	μ_b	κ_p	κ_b	η_s	η_N
1	6	35	300	7	0	0
2	6	35	30	7	0	0
3	6	5	0.03	3	0	0
4	3	10	0.03	0.1	0	0

For simplicity, damping is assumed by the same values $\eta_p = \eta_b = \eta_f$ and for the analysis of instability lines is gradually decreasing. Instability lines are shown in figures 4-5. Cases 1 and 2 are visualized in figure 4. These cases can be identified as regular, which is demonstrated by the asymptotic behaviour. In more details, it is seen that the vertical branches of the instability lines are tending to a fixed velocity ratio, which approaches the vertical line of the critical velocity of the moving force either from the left or from the right. The difference between cases 1 and 2 is that in case 1 there are three true critical velocities of the moving force, while in case 2 there is only one. When this happens, pseudocritical velocities must be determined, and the role of critical ones must be assigned to them. For figures 4-5, damping levels were assumed as 0.1, 0.05, $1 \cdot 10^{-4}$ and $1 \cdot 10^{-10}$. The lower the damping, the closer are the instability lines to the vertical lines, approaching them generally faster from the right than from the left. Assuming a specific, but relatively high moving mass ratio, three intervals of instability are detected, the last one being semi-infinite. For lower values, the first interval can be skipped, and the second interval can be divided in two, as it is seen in figure 4.

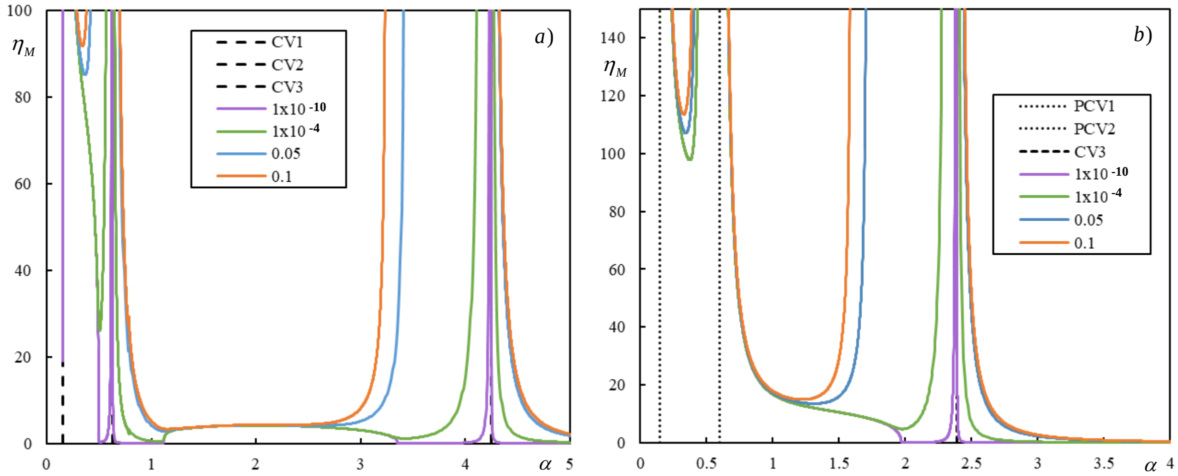

Figure 4. Instability lines: a) case 1; b) case 2. Damping is decreasing as indicated in the legend. Vertical lines indicate the critical velocity of the moving force (dashed – true, dotted – pseudo).

Cases 3 and 4 are plotted in figure 5. These cases are irregular, because the previous properties described above are not kept. It is seen that the instability lines can cross the vertical lines of the critical velocity of the moving force.

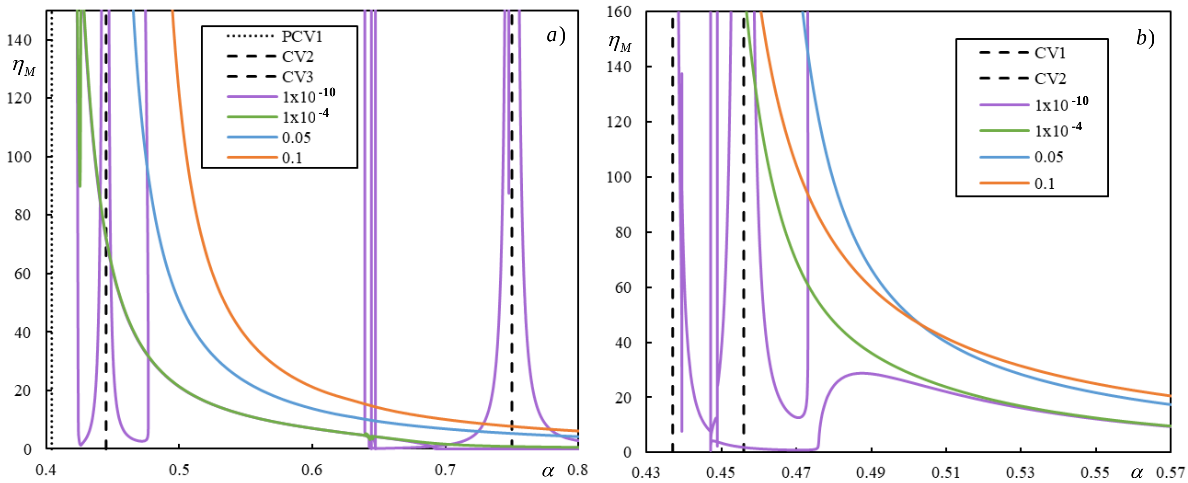

Figure 5. Instability lines: a) case 3; b) case 4. Damping is decreasing as indicated in the legend. Vertical lines indicate the critical velocity of the moving force (dashed – true, dotted – pseudo).

Both cases have two true values of such velocity. The third one must be completed by pseudocritical velocity. It is worthwhile to note, that in figure 5b) the pseudocritical velocity is not plotted. In fact, it should be there and then another branch of instability lines would be visible. However, this branch is only detected for quite low level of damping and very high, unrealistic for the assumed application, moving mass ratio. For this reason, it is not shown, and the horizontal scale is not covering this value. The irregularity of this case is demonstrated by crossing the vertical lines of the critical velocity and by strange additional branches that are revealed for very low damping levels. One of these curves is closed.

Pseudocritical velocities of the moving force can only be determined by a parametric analysis, which complicates their prediction. Moreover, unlike the true resonance, the extreme values can be attained at different velocity ratios, considering that the search is done on the values at the active point and also on the global maxima and minima over the full rail. In case 3, the pseudocritical velocity is well-defined, but in case 4 it is not, as demonstrated in figures 6 and 7. It is of note that there are other resonances, named as the false critical velocity. The maximum number of resonances for this model is five. When these values are compared with the analysis of finite beams, it is seen that some resonances identify a local maximum and not a local minimum, as it should be. In such cases the undamped steady-state solution does not exist, because it tends to infinity, but the properties of the true critical velocity are not fulfilled, as for instance, the sudden jump to zero deflection at the active point.

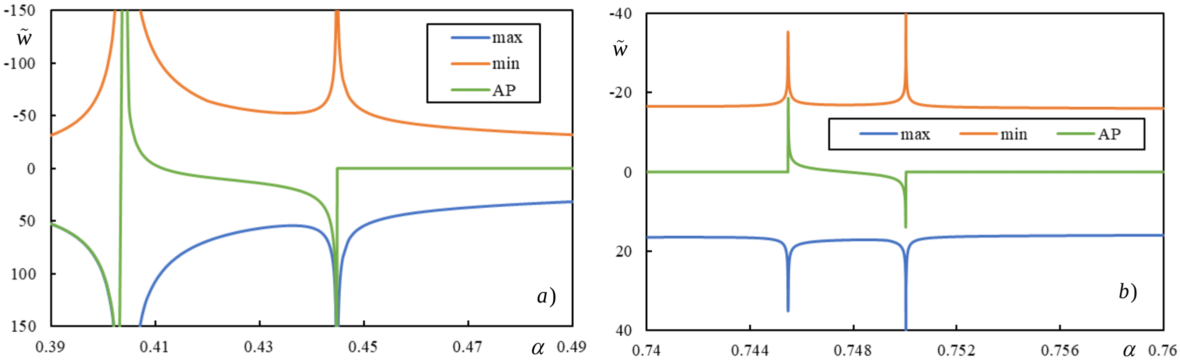

Figure 6. Parametric analysis of undamped steady state solution in case 3, parts a) and b) are showing different scales for better clarity. In the legend: max and min indicate the global maxima and minima over the full rail, AP indicates the value at the active point.

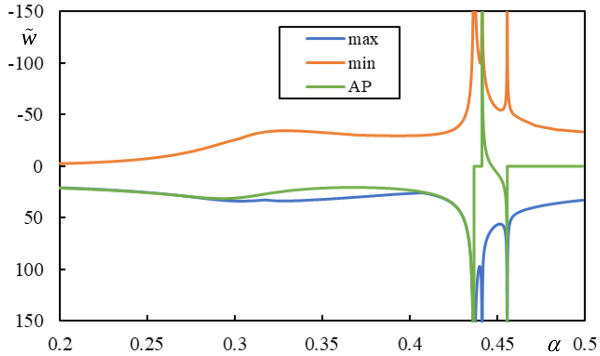

Figure 7. Parametric analysis of undamped steady state solution in case 4. In the legend: max and min indicate the global maxima and minima over the full rail, AP indicates the value at the active point.

Resonant values in case 3 are: 0.449, 0.745 and 0.750. The first and the last are the true critical velocities, the second one is the false one. The pseudocritical velocity at 0.404 is clearly visible, as such it is important for instability lines as demonstrated in figure 5a). In case 4, shown in figure 7, the resonant values are: 0.437, 0.442 and 0.456. Same as before, the first and the last are the true critical velocities, the second one is the false one. The pseudocritical velocity is not well-defined. There are two local extremes for the global maximum: 0.304 and 0.329; the local minimum is at 0.329 and the extreme at the active point is at 0.293, as can be concluded from figure 7.

Finally, it should be underlined that the instability of the moving mass is generated by the abnormal Doppler waves in the beam which appear when the mass velocity exceeds the minimum phase velocity of the waves. Particular situations described here in which the stability map has stable areas that alternate with unstable areas is not new, this being reported in other research works in the field [10]. Moreover, a similar situation can be encountered in the case of bogie hunting [26].

6. Conclusions

This paper compared application of two methods, the (semi)analytical and the Green's function method, applied on railway track model composed of three viscoelastic layers and used to determine the lowest possible velocity marking the separation between the stable and unstable behaviour of one uniformly moving mass. The model was simplified by assumption of continuous supports.

The semianalytical results were presented in form of so-called instability line, tracing the separation between the two regimes in the velocity-moving mass ratios plane. Such determination was supported by the exact evaluation of the K-function value, achieved by the precise contour integration method. Identification of instability lines was kept with the real domain. Additional calculations without damping necessary to determine the critical velocity of a moving force have been shown to cause no problems. Such values are important as they can affect the asymptotic behaviour of the instability lines. It was shown that the number of critical velocities determined analytically is not always complete and, in such cases, must be complemented by the pseudocritical velocities. It was further concluded that instability lines can have irregular behaviour, especially at low damping, showing several intervals of instability and difficult to predict in advance.

In the D-decomposition method, the critical velocity of the moving mass was determined using the Green’s function. It was demonstrated that all such values are identical with the ones determined by the semianalytical approach and there is thus no difference in accuracy between these two methods. However, in the D-decomposition method it was necessary to assume very low level of damping.

Acknowledgements
The work of the first author was supported by the Portuguese Foundation for Science and Technology (FCT), through IDMEC, under LAETA, project UIDB/50022/2020.
The work of the second author was supported by a grant of the Ministry of Research, Innovation and Digitization, CCCDI—UEFISCDI, project number PN-III-P2-2.1-PED-2021-0601, within PNCDI III.

References
[1] Duffy DG 1990 *J. Appl. Mech.* **57** 66–73
[2] Metrikine AV and Dieterman HA 1997 *J. Sound Vib.* **201** 567-576
[3] Stojanović V, Kozić P and Petković MD 2017 *Int. J. Solids Struct.* **108** 164–174
[4] Dimitrovová Z 2021 *Appl. Math. Modell*. **100** 192-217
[5] Dimitrovová Z 2022 *Int. J. Mech. Sci*. **217** 107042
[6] Metrikine AV, Verichev SN and Blaauwendraad J 2005 *Int. J. Solids Struct*. **42** 1187–1207
[7] Stojanović V, Petković MD and Deng J 2019 *Eur. J. Mech. A/Solids* **75** 367–380
[8] Verichev SN and Metrikine AV 2002 *J. Sound Vib.* **253** 653-668
[9] Stojanović V, Deng J, Petković M and Milić D 2023 *Eng. Struct*. **295** 116788
[10] Mazilu T 2013 *J. Sound Vib.* **332** 4597–4619
[11] Yang B, Gao H and Liu S 2018 *Int. J. Struct. Stab. Dyn.* **18** 1850125
[12] Roy S, Chakraborty G and DasGupta A 2018 *J. Sound Vib.* **415** 184–209
[13] Nassef ASE, Nassar MM and EL-Refaee MM 2019 *Iran. J. Sci. Technol. Trans. Mech. Eng.* **43** 419–426
[14] Stojanović V, Petković M and Deng J 2018 *Eur. J. Mech. A. Solids*. **69** 238-254
[15] Stojanović V, Deng J, Milić D and Petković MD 2024 *J. Sound Vib.* **570** 118020
[16] Metrikine AV 1994 *Acoust. Phys*. **40** 85–89
[17] Dimitrovová Z 2023 *Vibration* **6** 113-146
[18] Dimitrovová Z and Mazilu T 2024 *Materials* **117** 279
[19] Yang CJ, Xu Y, Zhu WD, Fan W, Zhang WH and Mei GM 2020 *J. Sound Vib.* **479** 115363
[20] Abea K, Chidaa Y, Quinay PEB and Koroa K 2014 *J. Sound Vib.* **333** 3413–3427
[21] Koh CG, Ong JSY, Chua DKH and Feng J 2003 *Int. J. Numer. Methods Eng.* **56** 1549–1567
[22] Ang KK and Dai J 2013 *J. Sound Vib.* **332** 2954–2970
[23] Xu Y, Zhu W, Fan W, Yang C and Zhang W 2020 *J. Vib. Acoust. Trans. ASME* **142** 031001
[24] Elhuni H and Basu D 2021 *ASCE J. Eng. Mech.* **147** 04021012
[25] Jahangiri A, Attari NKA, Nikkhoo A and Waezi Z 2020 *Arch. Appl. Mech.* **90** 1135–1156
[26] Wickens A H 2003 *Fundamentals of Railway Vehicle Dynamics* (CRC Press)